Am J Transl Res 2026;18(3):1808-1825
www.ajtr.org /ISSN:1943-8141/AJTR0168975

Original Article

Gypenosides attenuate H_2O_2-induced oxidative stress in orbital fibroblasts from thyroid-associated ophthalmopathy by activating the Nrf2/ERK/HO-1 signaling pathway

Chao Ma[1], Kaijun Li[2], Haoyu Li[3], Xinmin Li[4], Wei Liu[2], Xian Li[5], Jinyuan Chen[6]

[1]Department of Ophthalmology, The First Affiliated Hospital of Zhengzhou University, Zhengzhou 450052, Henan, China; [2]Department of Ophthalmology, The First Affiliated Hospital of Guangxi Medical University, Nanning 530021, Guangxi Zhuang Autonomous Region, China; [3]Department of Ophthalmology, The Second Xiangya Hospital, Central South University, Changsha 410011, Hunan, China; [4]Department of Ophthalmology, The First Affiliated Hospital of Xinxiang Medical University, Xinxiang 453100, Henan, China; [5]Faculty of Biology, University of Manchester, Manchester M13 9PL, England, United Kingdom; [6]Department of Ophthalmology, The First Affiliated Hospital of Fujian Medical University, Fuzhou 350005, Fujian, China

Received September 23, 2025; Accepted February 5, 2026; Epub March 15, 2026; Published March 30, 2026

Abstract: Objectives: To explore the antioxidative effects of gypenosides (Gyps) in orbital fibroblasts (OFs) derived from patients with thyroid-associated ophthalmopathy (TAO) and to validate their therapeutic efficacy *in vivo* using an animal model. Methods: Bioinformatics analyses were performed to screen potential genes and signalling pathways underlying the effect of Gyps in OFs. OFs were isolated from orbital connective tissues of both TAO patients and non-TAO controls. CCK-8 assay was used to detect cell proliferation. Oxidative stress was evaluated by measuring reactive oxygen species (ROS) and superoxide dismutase (SOD) levels. Quantitative reverse transcriptive-polymerase chain reaction (RT-qPCR), ELISA, and western blotting were employed to ascertain the effects of Gyps on H_2O_2-induced oxidative stress, inflammation, fibrosis, and autophagy. Furthermore, a TAO mouse model was established. Gyps were administered by intraperitoneal injection (50 mg/kg/day for 4 weeks) to evaluate their protective effects against oxidative stress, inflammation, and fibrosis in orbital tissues. Results: Bioinformatic analysis revealed that the identified genes were primarily enriched in metabolic and oxidative stress-related pathways. *In vitro* experiments demonstrated that Gyps significantly reduced H_2O_2-induced ROS generation, increased SOD levels, and suppressed the expression of inflammation-, fibrosis-, and autophagy-related markers. These effects were associated with the activation of the nuclear factor erythroid 2-related factor 2 (Nrf2)/extracellular-regulated kinase (ERK)/heme oxygenase 1 (HO-1) pathway. *In vivo* animal experiments further confirmed that Gyps treatment effectively alleviated oxidative injury, inflammatory cell infiltration, and collagen deposition in the orbital tissues of TAO model mice. Conclusions: Gyps exert significant antioxidative, anti-inflammatory, and anti-fibrotic effects by activating the Nrf2/ERK/HO-1 signalling pathway in both *in vitro* and *in vivo* TAO models.

Keywords: Gypenosides, orbital fibroblast, thyroid-associated ophthalmopathy, oxidative stress, bioinformatics, animal models

Introduction

Thyroid-associated ophthalmopathy (TAO) is an autoimmune disorder associated with thyroid dysfunction, particularly hyperthyroidism and is characterized by excessive thyroid hormone release [1]. About 25-30% of TAO cases are secondary to Graves's hyperthyroidism, making TAO the most common extrathyroidal manifestation of autoimmune thyroid disease [2, 3].

The pathogenesis of TAO is complex and involves a dysregulated immune response within the orbit. Orbital fibroblasts (OFs) are exposed to inflammatory mediators released by infiltrating immune cells, including neutrophilic T lymphocytes, B lymphocytes, macrophages, and mast cells. Importantly, OFs express key surface receptors implicated in TAO, such as the thyroid stimulating hormone receptor (TSHR) and the insulin like growth factor 1 receptor

https://doi.org/10.62347/ABZG4110

(IGFR) [4, 5]. Activation of these receptors triggers the pathologic processes, including fibroblast proliferation, inflammatory mediator release, extracellular matrix synthesis, fatty acid production, and the development of fibrosis [6, 7]. Alterations in OFs play a pivotal role in the initiation and progression of TAO and represent a promising therapeutic target.

Multiple pathogenic mechanisms affect the course of TAO, resulting in orbital tissue remodeling and intra-orbital pressure-related pathologic changes [8]. One of the underlying mechanisms is the release of reactive oxygen species (ROS). Excessive ROS production and impaired antioxidant defense may result in oxidative stress and subsequent cellular damage [9]. Therefore, oxidative stress represents a critical contributor to the development of TAO and other orbital diseases.

Current research identifies OFs as the primary effector cells in TAO lesions, and these cells not only proliferate but also differentiate into myofibroblasts and adipocytes, contributing to fibrosis and fat expansion within the orbit [10]. In addition, OFs can produce extracellular matrix components (especially glycosaminoglycans) and interact with monocytes. Moreover, OFs continuously secrete inflammation-related chemokines and cytokines to sustain chronic orbital inflammation in TAO patients [11]. Interleukin-1β (IL-1β) and leukocyte regulatory proteins can significantly increase hyaluronic acid (HA) secretion by OFs, while transforming growth factor-β1 (TGF-β) expression is also upregulated under the stimulation of cytokines and growth factors [12]. Therefore, OFs function as central effector cells in orbital lesions primarily through the secretion of inflammatory and fibrotic factors.

Gynostemma pentaphyllum is a natural plant extract widely used to treat chronic inflammation, atherosclerosis, hyperlipidemia, and liver diseases in Asian countries [13]. Gypenosides (Gyps), the major bioactive components of *Gynostemma pentaphyllum*, comprise more than 100 identified saponin compounds [14-16]. Previous studies have shown that Gyps possess neuroprotective, antioxidant, antifibrotic, and anti-inflammatory properties [17, 18]. Notably, Gyps exhibit strong antioxidative activity by effectively scavenging ROS [19, 20]. Furthermore, long-term *in vivo* administration of Gyps has been shown to be safe and nontoxic, and evidence supports their therapeutic potential in various chronic diseases [21, 22].

However, the role of Gyps in regulating oxidative stress-induced inflammation and fibrosis in orbital fibroblasts remains unclear. Therefore, this study aimed to investigate whether Gyps could attenuate inflammation and fibrosis induced by oxidative stress (OxS) in OFs and to elucidate the underlying molecular mechanisms, through with a particular focus on the nuclear factor erythroid 2-related factor 2 (Nrf2)/extracellular signal-regulated kinase (ERK)/heme oxygenase-1 (HO-1) signaling pathway [23, 24].

Materials and methods

Bioinformatic analysis for Gyps on treating TAO

All saponin components of *Gynostemma pentaphyllum* were retrieved from the Traditional Chinese Medicine Systems Pharmacology Database and Analysis Platform (TCMSP; http://lsp.nwu.edu.cn/tcmsp.php) [25]. PharmMapper (http://www.lilab-ecust.cn/pharmmapper/submitfile.html) was used for predicting potential therapeutic targets for each saponin, which were merged for further analysis [26-28]. A pharmacophore mapping approach was employed to determine possible target candidates for each saponin.

TAO-related target genes were obtained by intersecting results from three databases: the Online Mendelian Inheritance in Man database (OMIM, https://www.omim.org/), GeneCards Human gene database (https://www.genecards.org/), and Comparative Toxicogenomic Database (CTD, http://ctd.mdibl.org/). Searches were performed using the keywords of *thyroid-associated ophthalmopathy* and *Graves' ophthalmopathy*. Then, the online Venny tool (http://bioinfogp.cnb.csic.es/Tools/Venny/index.html) was used to identify overlapping targets between Gyps- and TAO-related genes.

To elucidate the potential biological processes and signaling pathways involved in the therapeutic effects of Gyps on TAO, Database for Annotation, Visualization and Integrated Discovery (DAVID) v6.8 (https://david.ncifcrf.gov/) was used for the Kyoto Encyclopedia of Genes and Genomes (KEGG) pathway and Gene

Table 1. Clinical characteristics of TAO and non-TAO patients included in this study

Age (years)	Sex	Smoker	Duration of TAO (years)	CAS	Proptosis R/L (mm)	Surgical treatment
TAO subjects						
61	Female	no	0.5	0/7	21/20	Decompression
48	Female	no	0.5	1/7	20/22	Decompression
52	Female	no	1	1/7	19/21	Decompression
57	Male	no	20	1/7	23/23	Decompression
Non-TAO subjects						
35	Female	no	n/a	n/a	n/a	Eye evisceration
21	Male	no	n/a	n/a	n/a	Eye evisceration
50	Male	yes	n/a	n/a	n/a	Eye evisceration
33	Female	no	n/a	n/a	n/a	Upper lid blepharoplasty

TAO, thyroid-associated ophthalmopathy; CAS, clinical activity score; n/a, not applicable; R, right eye; L, left eye.

Ontology (GO) enrichment analyses [29, 30]. In addition, a protein-protein interaction (PPI) network was constructed using the STRING database (https://string-db.org/) based on the intersecting target genes. An interaction confidence score of 0.10 was set as the threshold, and isolated nodes were excluded from the network. Cytoscape v3.6.1 software was used to visualize the PPI network, with node size and color representing topological indicators.

Reagents and patients

Gyps (purity ≥98%) were purchased from Xi'an Jiatian Biotechnology Co., Ltd. (China). Hydrogen peroxide (H_2O_2, 3%) was obtained from Millipore (USA). Dulbecco's modified Eagle's medium (DMEM), fetal bovine serum (FBS), penicillin, and streptomycin were purchased from Invitrogen (California, USA). The Cell Counting Kit-8 (CCK-8) assay kit was obtained from Beyotime Biotechnology (Shanghai, China). PCR kits were purchased from Takara (Dalian, China). ELISA kits for IL-1β, IL-6, INF-γ and TNF-α were obtained from MultiSciences (Hangzhou, China). Antibodies against α-smooth muscle actin (α-SMA) and fibronectin (FN) were obtained from Lianshuo Biotechnology (Shanghai, China). Collagen I (Col I) and hyaluronic acid (HA) ELISA kits were obtained from Enzyme-linked Biotechnology (Shanghai, China). ROS and superoxide dismutase (SOD) kits were supplied by Solarbio (Beijing, China). Primary antibodies against HO-1, ERK1/2, phospho-ERK1/2, Nrf2, and β-actin were all purchased from Cell Signaling Technology (Massachusetts, USA).

Orbital connective tissues were obtained from four patients with TAO patient (three females and one male; mean age 54.50 years; range 48-61 years). Normal control tissues were collected from four patients (two females and two males; mean age 34.75 years; range 21-50 years) who underwent eyeball enucleation due to corneal staphyloma or upper eyelid blepharoplasty without a history of thyroid disease. The clinical features of all subjects are shown in **Table 1**. All procedures were conducted in accordance with the Helsinki Declaration and were approved by the Ethics Review Committee of the First Affiliated Hospital of Guangxi Medical College (2019[KY-E092]). Written informed consent was obtained from all participants. All TAO patients were in a stable thyroid function state and had discontinued glucocorticoids for at least 6 months prior to surgery. The 7-point Clinical Activity Score (CAS) of all patients during surgery was less than 3, indicating an inactive inflammatory state [31].

Cell culture

OFs were isolated from the orbit connective tissues and cultured. Briefly, the harvested tissue was finely minced, the visible vascular tissue was removed. The tissue fragments were washed with phosphate buffered saline (PBS), and then placed in a plastic petri dish containing DMEM/F12 (1:1) supplemented with 20% FBS, penicillin (100 U/ml), and streptomycin (0.1 mg/ml). Fibroblasts were allowed to migrate out of the tissue explants and proliferate. After sufficient outgrowth, the fibroblasts were gently detached using trypsin-ethylenediamine-

Table 2. Primer sequences used for RT-qPCR

Gene	Forward primers 5'-3'	Reverse primers 5'-3'
IL-1β	CTGAGCTCGCCAGTGAAATG	TGTCCATGGCCACAACAACT
IL-6	AAGCCAGAGCTGTGCAGATGAGTA	TGTCCTGCAGCCACTGGTTC
TNF-α	CTGCCTGCTGCACTTTGGAG	ACATGGGCTACAGGCTTGTCACT
IFN-γ	CACTGCATCTTGGCTTTGCA	GCTGATGGCCTGATTGTCTTTC
α-SMA	CTCTGGACGCACAACTGGCATC	CACGCTCAGCAGTAGTAACGAAGG
HA	CACGTAACGCAATTGGTCTTGTCC	CCAGTGCTCTGAAGGCTGTGTAC
Col-1	CTGGACCTCCAGGTGTAAGC	TGGCTGAGTCTCAAGTCACG
FN	ACAAGCATGTCTCTCTGCCA	TTTGCATCTTGGTTGGCTGC
GAPDH	GACAGTCAGCCGCATCTTCT	GCGCCCAATACGACCAAATC

RT-qPCR, quantitative reverse transcriptive-polymerase chain reaction; IL-1β, interleukin-1β; IL-6, interleukin-6; TNF-α, tumor necrosis factor-α; IFN-γ, interferon-γ; α-SMA, α-smooth muscle actin; HA, hyaluronic acid; Col-1, collagen 1; FN, fibronectin; GAPDH, glycera ldehyde-3-phosphate dehydrogenase.

tetraacetic acid (EDTA) and sub-cultured as a monolayer in a 25-cm^2 culture flask containing DMEM/F12 supplemented with 10% FBS and antibiotics. The cells were cultured in a humidified incubator with 5% CO_2 at 37°C. Excess cells were stored in liquid nitrogen and thawed for subsequent experiments when needed. OFs between passages 2 and 6 were used for experiments.

Proliferation assay

Cell proliferation was assessed using the CCK-8 assay. OFs were seeded into 96-well plates at a density of 6.0×10^3 cells per well and allowed to adhere overnight. To determine the optimal concentrations, cells were exposed to various concentrations of H_2O_2 (0, 2.5, 5, 10, 50, and 100 μM) for 24 h or to different concentrations of Gyps (0, 25, 50, 100, 250, 500, and 1000 μg/mL) for 48 h. After treatment, cells were rinsed with PBS, and CCK-8 regent was added to each well, followed by incubation at 37°C for 3.5 h. absorbance was measured at 450 nm using a full-wavelength microplate reader. All experiments were performed in triplicate.

RT-qPCR

Total RNA was extracted from OFs using TRIzol reagent according to the manufacturer's instructions. Complementary DNA (cDNA) was synthesized using a reverse transcription kit. RT-qPCR was performed using SYBR PreMix Ex TaqII on an ABI 7500 real-time PCR system (CA, USA).

Gene expression levels of IL-6, IL-1β, TNF-α, IFN-γ, α-SMA, COL1A2, HAS2, FN1, LC3, BECN1, and GAPDH were quantified using gene-specific primers (**Table 2**). The PCR conditions were as follows: initial denaturation at 95°C for 30 s, followed by 40 cycles of denaturation at 95°C for 5 s and annealing/extension at 60°C for 34 s. Relative gene expression levels were normalized to GAPDH and calculated using the $2^{-\Delta\Delta Ct}$ method relative to the control group. Only data with Ct values < 35 were included in the analysis. All experiments were performed in triplicate.

ELISA

Cell culture supernatants were collected according to the instructions. The supernatants were centrifuged to remove cellular debris and then stored at -80°C until further analysis. The concentrations of α-SMA, FN, Col I, TNF-α, IL-1β, IL-6, HA, and IFN-γ were quantified using commercial ELISA kits. Absorbance was measured at 450 nm using a full-wavelength microplate reader. Each sample was assayed in triplicate.

Measurement of ROS and SOD

Intracellular ROS levels were measured using the fluorescent probe 2',7'-dichlorodihydrofluorescein diacetate (DCFH-DA). After pretreatment with Gyps and H_2O_2 as per manufactures instructions, cells were digested, collected, and resuspended in serum-free medium. DCFH-DA was added to a final concentration of 10 μM, and cell density was adjusted to 1×10^6 cells/ml. Cells were incubated at 37°C for 30 minutes, and then gentle mixed every 3 min. After incubation, cells were washed 3 times with serum-free medium. Fluorescence intensity was measured using a microplate reader at an excitation wavelength of 488 nm and an emission wavelength of 525 nm.

SOD activity was measured using a SOD kit according to the manufacturer's instructions. Briefly, $1.0*10^6$ cells were collected after cen-

trifugation, and the supernatant was discarded. Cell lysis buffer (200 μl per 5.0×10^7 cells) was added, and then cells were disrupted by ultrasonic homogenization (power 20% or 200 W, ultrasound 3 s, pause 10 s, repeated 30 times). The supernatant was centrifuged at 8,000×g for 10 minutes at 4°C before collection for analysis. Subsequently, 200 μl of reaction reagent was added to each well of a 96-well plate, and absorbance was measured at 560 nm. All experiments were performed three times.

Western blotting assay

OFs were pretreated with Gyps (100 μg/ml) for 24 hours and then stimulated with 5 μM H_2O_2 (5 μM) for additional 24 hours. After washing with PBS, cells were lysed on ice for 30 minutes using lysis buffer containing 50 mM Tris (pH 7.4), 150 mM NaCl, 1% Triton X-100, 1% sodium deoxycholate, 0.1% sodium dodecyl sulfate (SDS) and EDTA. Cell lysates were centrifuged to obtain total protein extracts. Equal amounts of protein were separated by 10% SDS-PAGE electrophoresis and transferred to polyvinylidene fluoride (PVDF) membranes. After blocking the nonspecific binding with blocking buffer at room temperature for 1 hour, the primary antibody was diluted with TBST and incubated overnight. After washing, membranes were incubated with fluorescent secondary antibodies at room temperature for 2 hours in the dark. Protein bands were visualized and quantified using the Odyssey two-colour infrared fluorescence imaging system.

Establishment of the TAO animal model and in vivo Gyps intervention

All animal experiments were reviewed and approved by the Institutional Animal Care and Use Committee and were conducted strictly in accordance with national and international regulations on the use and care of laboratory animals.

Twenty C57BL/6 mice were randomly divided into four groups (n = 5 per group): control group, TAO mode group, TAO + low-dose Gyps group (25 mg/kg), TAO + high-dose Gyps group (50 mg/kg). TAO model was induced by intramuscular injection of a viral vector expressing the human TSHR α-subunit. Following successful model establishment, mice in the Gyps treatment groups received daily intraperitoneal injection of Gyp at the indicated doses for 4 weeks. Mice in the control and model groups received an equal volume of normal saline via intraperitoneal injection. At the end of the intervention period, mice were euthanized by intraperitoneal injection of an overdose of sodium pentobarbital or by inhalation of an overdose of isoflurane. Orbital tissues were harvested from the mice. Part of the tissue was fixed in 4% paraformaldehyde for histologic analysis, and the rest was kept at -80°C for subsequent molecular analyses.

Histologic and immunohistochemical analysis

Fixed orbital tissues were paraffin-embedded, sectioned, and subjected to H&E staining to assess inflammatory cell infiltration. Masson's trichrome staining was performed to evaluate collagen deposition and the degree of fibrosis. Concurrently, immunohistochemical staining was performed using antibodies against Nrf2, HO-1, and α-SMA to semi-quantitatively analyze the expression and localization of these proteins within orbital tissues.

Statistical analyses

All experiments were conducted independently at least three times, and cell experiments were conducted using cells from at least three different donors. Data were analyzed using GraphPad Prism software (Windows v8.2.0, San Diego, USA). Data were expressed as mean ± standard deviations (SD). Comparisons among multiple groups were performed using one-way analysis of variance (ANOVA), followed by appropriate post hoc tests. A P value < 0.05 was considered significant (*P < 0.05; **P < 0.01; ***P < 0.001; ****P < 0.0001).

Results

Bioinformatics analysis

'*Gynostemmae Pentaphylli Herba*' was searched in the TCMSP database, and a total of 103 saponin components were obtained. After prediction, 20 candidate targets were identified for each saponin, and 157 unique targets were ultimately obtained after merging and removing duplicates. The OMIM, CTD and GeneCard databases were searched to collect TAO-related targets, yielding a total of 1,851

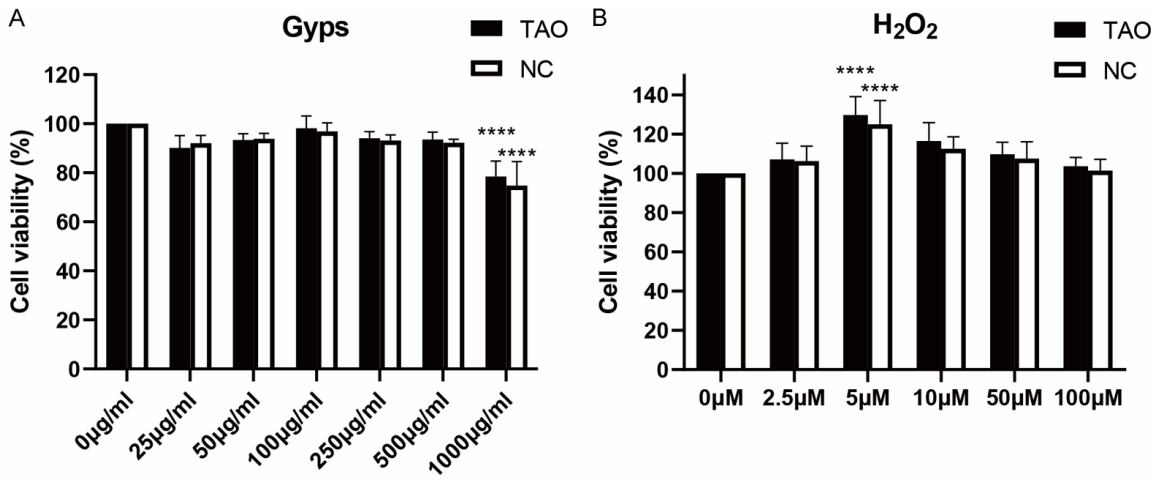

Figure 1. Effects of Gyps (A) and H_2O_2 (B) on the viability of orbital fibroblasts derived from TAO and non-TAO patients. Orbital fibroblasts were treated with Gyps (48 hours) and H_2O_2 (24 hours) at desired concentrations. ****P < 0.0001, compared to 0 ug/ml. Gyps, gypenosides; TAO, thyroid-associated ophthalmopathy; NC, non-TAO control.

TAO-associated genes. Intersection analysis identified 32 overlapping targets, which were subjected to subsequent analyses (Figure S1).

GO enrichment analysis revealed that, among biological processes (BP), the intersecting targets were mainly enriched in the redox-related processes, including oxidation-reduction processes (GO:0055114), response to decreased oxygen levels (GO:0036293), and response to oxygen levels (GO:0070482). In the cellular component (CC) category, these targets were predominantly localized in the cytoplasmic part (GO:0044444), mitochondria (GO:0005739) and endoplasmic reticulum (GO:0044432). Molecular function (MF) analysis indicated significant enrichment in oxidoreductase activity (GO:0016491), antioxidant activity (GO:0016209), oxidoreductase activity acting on the CH-CH group of donors (GO:0016627), oxidoreductase activity acting on the CH-OH group of donors with NAD or NADP as acceptor (GO:0016616) (Figure S2). Pathway analysis using KEGG and REACTOME databases demonstrated that the targets were mainly enriched in metabolic pathways and cellular responses to external stimuli, particularly oxidative stress (Figure S3).

A PPI network revealed interactions among the intersecting targets, with SOD2 identified as a central node exhibiting a high interaction score (Figure S4).

Effects of Gyps and H_2O_2 on OF proliferation assessed by CCK-8 assay

The CCK-8 assay was used to detect the effects of different concentrations of Gyps on cell proliferation of OFs derived from TAO patients and non-TAO controls. After 48 hours of treatment, cell viability in both groups decreased significantly at 1,000 μg/ml. In contrast, cell activity was the highest at a Gyps concentration of 100 μg/ml and did not exceed that of the PBS-treated control group (**Figure 1A**). Therefore, 100 μg/ml was selected as the optimal concentration for subsequent experiments. To establish an appropriate oxidative stress model, OFs were treated with different concentrations of H_2O_2 for 24 h. Cell viability increased with rising H_2O_2 concentrations and peaked at 5 μM, followed by a decline at higher concentrations (**Figure 1B**). Therefore, 5 μM H_2O_2 was selected for subsequent experiments.

Gyps inhibited H_2O_2-induced inflammation and fibrosis in OFs

The effects of Gyps on H_2O_2 induced inflammation and fibrosis were detected by RT-qPCR and ELISA. Following stimulation with 5 μM H_2O_2 for 24 h, the mRNA expression levels of inflammatory cytokines (IL-1β, IL-6, TNF-α, and IFN-γ) and fibrosis-related markers (α-SMA, HA, Col-I, and FN) were significantly upregulated in primary OFs (**Figure 2**).

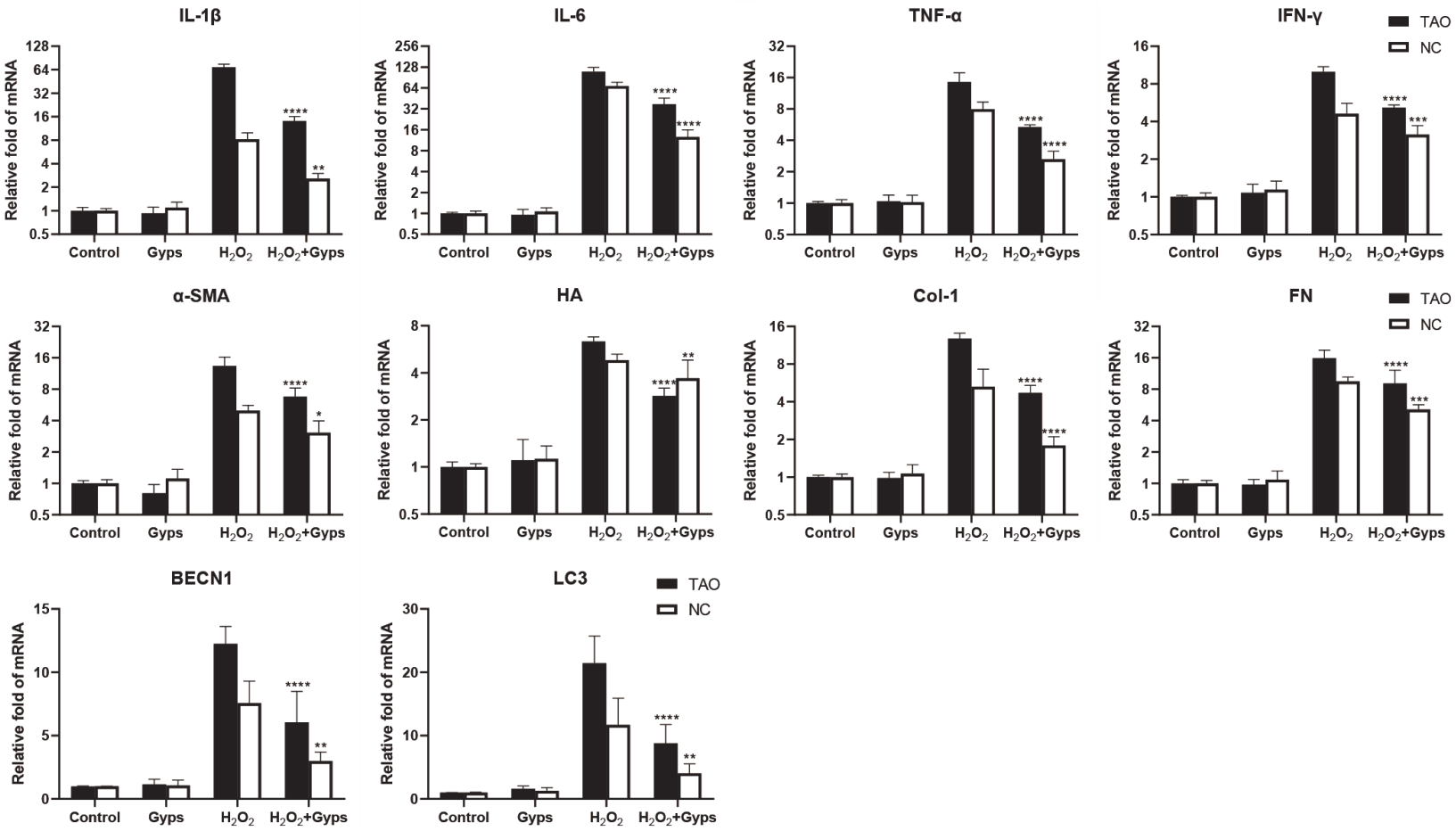

Figure 2. Effects of Gyps on the mRNA expression of *IL-1β*, *IL-6*, *TNF-α*, *IFN-γ*, *α-SMA*, *HA*, *Col-1*, *FN*, *LC3* and *BECN1* in orbital fibroblasts from derived from TAO and non-TAO patients determined by RT-qPCR. Orbital fibroblasts from TAO (n = 4) and non-TAO patients (n = 4) were treated with 5 μM H_2O_2 for 24 hours in the absence or presence of Gyps pretreatment (100 μg/ml, 24 hours). Orbital fibroblasts without any interventions served as the Control group. No significant differences were observed between the Control group and Gyps group (all $P > 0.05$). H_2O_2 (5 μM, 24 hours) treatment significantly increased the expression of above mRNA than Controls ($P < 0.0001$). The above indexes in the cells pretreated with Gyps were lower than those in the H_2O_2 group ($P < 0.05$). *$P < 0.05$, **$P < 0.01$, ***$P < 0.001$, ****$P < 0.0001$, compared to the H_2O_2 group. Gyps, gypenosides; TAO, thyroid-associated ophthalmopathy; IL-1β, interleukin-1β; IL-6, interleukin-6; TNF-α, tumor necrosis factor-α; IFN-γ, interferon-γ; α-SMA, α-smooth muscle actin; HA, hyaluronic acid; Col-1, collagen 1; FN, fibronectin; BECN1, microtubule-associated protein Beclin1; LC3, microtubule-associated protein light chain 3.

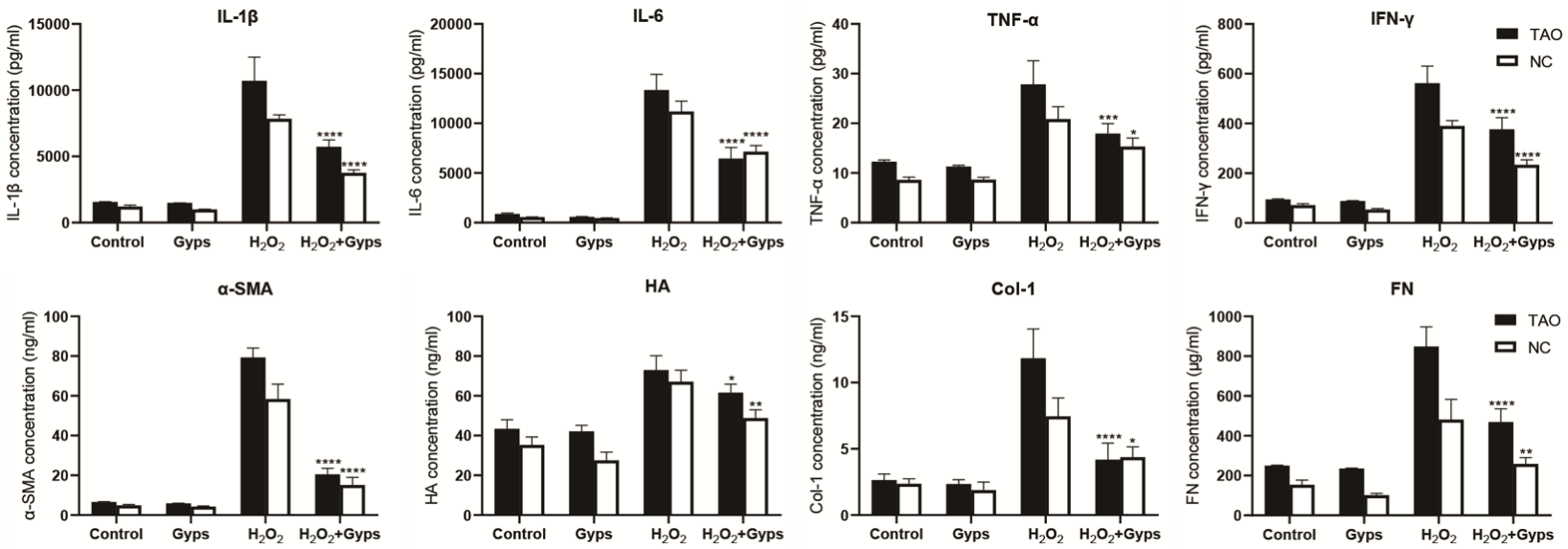

Figure 3. Effects of Gyps on the production of pro-inflammatory cytokines and fibrosis-related proteins in orbital fibroblasts from TAO and non-TAO patients by ELISA. Orbital fibroblasts from TAO (n = 4) and non-TAO patients (n = 4) were treated with H_2O_2 (5 μM, 24 hours) in the absence or presence of Gyps pretreatment (100 μg/ml, 24 hours). Orbital fibroblasts without any interventions served as the Control group. No significant differences were observed between Control group and Gyps group (all $P > 0.05$). H_2O_2 (5 μM, 24 hours) treatment significantly increased the expression of IL-1β, IL-6, TNF-α, IFN-γ, α-SMA, HA, Col-1, and FN ($P < 0.0001$). Pretreatment with Gyps had an inhibitory effect on IL-1β, IL-6, TNF-α, IFN-γ, α-SMA, HA, Col-1, and FN ($P < 0.05$). *$P < 0.05$, **$P < 0.01$, ***$P < 0.001$, ****$P < 0.0001$, compared with the H_2O_2 group. Gyps, gypenosides; ELISA, enzyme linked immunosorbent assay; TAO, thyroid-associated ophthalmopathy; IL-1β, interleukin-1β; IL-6, interleukin-6; TNF-α, tumor necrosis factor-α; IFN-γ, interferon-γ; α-SMA, α-smooth muscle actin; HA, hyaluronic acid; Col-1, collagen 1; FN, fibronectin.

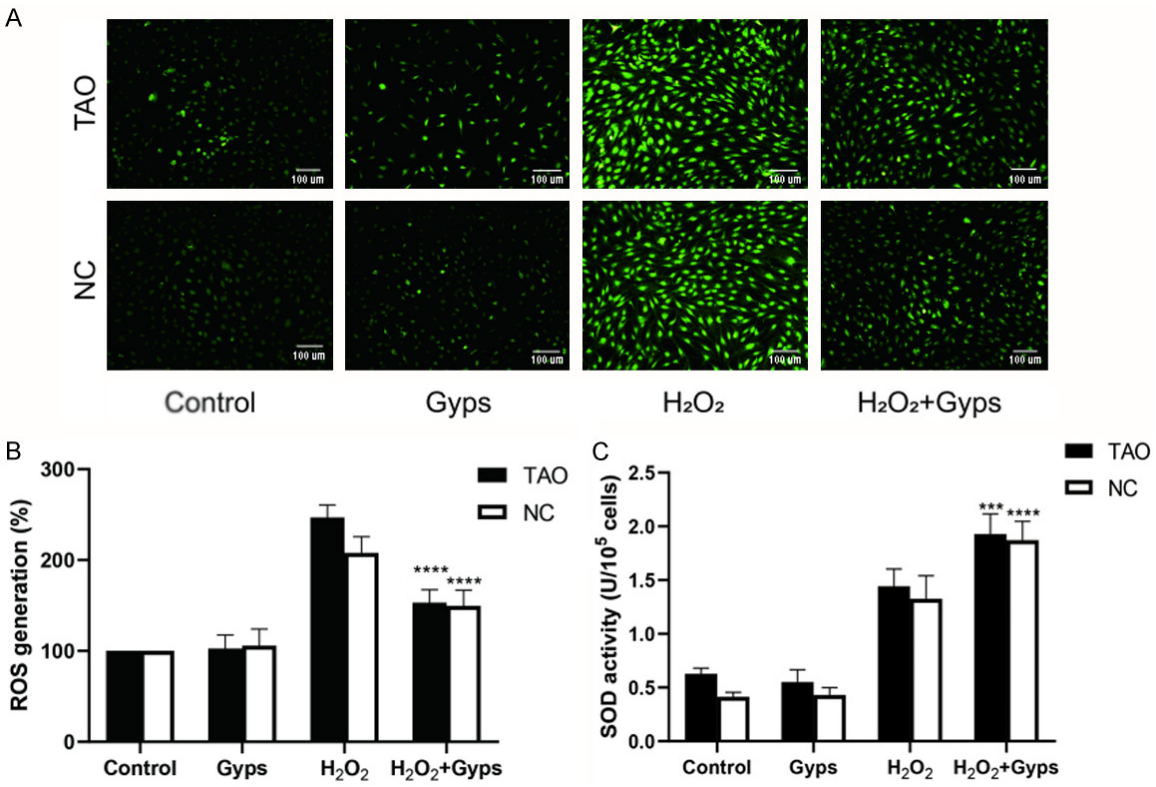

Figure 4. Effects of Gyps on oxidative stress in orbital fibroblasts from TAO and non-TAO patients (×10). A. Representative fluorescence microscopy images showing ROS levels detected using DCFDA staining. B. Quantitative analysis of ROS fluorescence intensity. C. Quantitative analysis of SOD activity. No significant differences in ROS and SOD content were observed between the Control group and Gyps group (all $P > 0.05$). H_2O_2 (5 μM, 24 hours) treatment significantly increased the expression of SOD ($P < 0.0001$). The activity of ROS treated with H_2O_2 (5 μM, 24 hours) and Gyps (100 μg/ml, 24 hours) was lower than in cells treated with H_2O_2 alone ($P < 0.001$); The activity of SOD was higher than in cells treated with H_2O_2 alone ($P < 0.001$). ***$P < 0.001$, ****$P < 0.0001$, compared with the H_2O_2 group. ROS, reactive oxygen species; DCFDA, 2',7'-Dichlorodihydrofluorescein diacetate; Gyps, gypenosides; TAO, thyroid-associated ophthalmopathy; NC, non-TAO control; SOD, superoxide dismutase.

In addition, the protein levels of IL-1 β, IL-6, and TN F-α in the culture supernatants were increased after H_2O_2 stimulation, along with elevated levels of α-SMA, HA, Col I, and FN (**Figure 3**). Furthermore, pre-treatment with Gyps (100 μg/ml, 24 h) significantly inhibited both the mRNA and protein secretion of inflammation- and fibrosis-related markers induced by H_2O_2.

Gyps attenuated H_2O_2-induced oxidative stress in OFs

To determine whether Gyps exert antioxidant effects in OFs, intracellular ROS levels were assessed using the ROS-sensitive fluorescent probe DCFDA. Fluorescence imaging demonstrated a marked increase in ROS accumulation following H_2O_2 stimulation demonstrated a marked increase in ROS accumulation following H_2O_2 stimulation, whereas Gyps pretreatment for 24 h significantly reduced ROS accumulation (**Figure 4A**, **4B**). In parallel, SOD activity was markedly decreased following H_2O_2 exposure but was significantly restored by Gyps pretreatment (**Figure 4C**).

Gyps mediated oxidant stress by the Nrf2/ERK/HO-1 signaling pathway

Western blot analysis showed that H_2O_2 stimulation significantly increased the protein levels of Nrf2 and HO-1 compared to the control group ($P < 0.01$; **Figure 5**), consistent with activation of inflammation, fibrosis, and oxidative stress markers. Notably, Gyps pretreatment further enhanced the expression of Nrf2 and HO-1 compared to H_2O_2 treatment ($P < 0.05$).

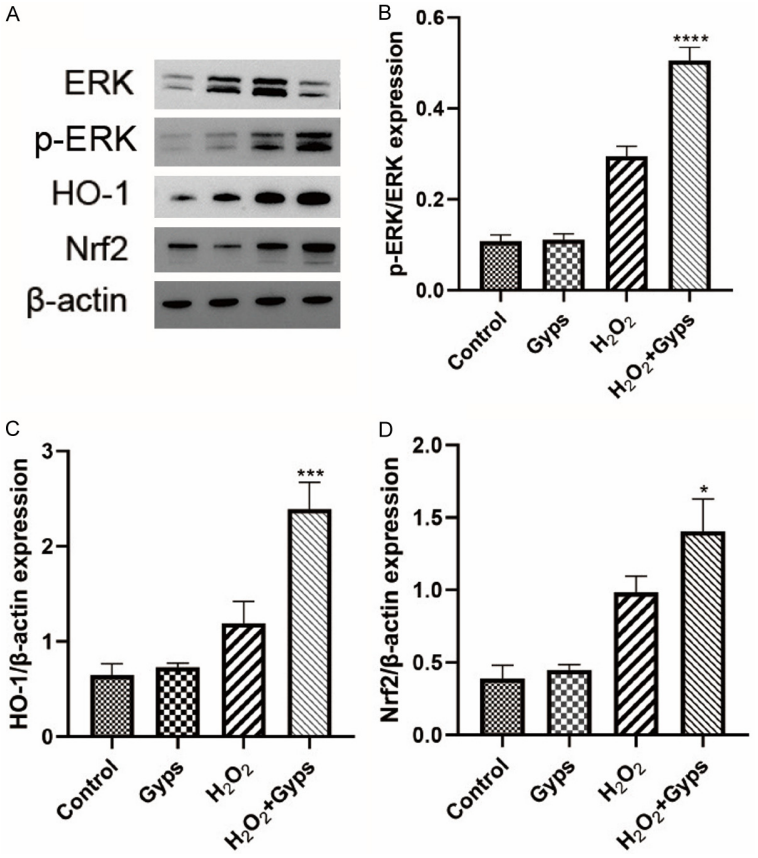

Figure 5. Gyps promoted activation of the Nrf2/ERK/HO-1 signaling pathway in orbital fibroblasts from TAO patients. A. Representative blot images of p-ERK, HO-1, and Nrf2. B. Quantitative analysis of p-ERK. C. Quantitative analysis of HO-1. D. Quantitative analysis of Nrf2. Orbital fibroblasts from TAO patients (n = 4) were treated with H_2O_2 (5 μM, 24 hours) in the absence or presence of Gyps pretreatment (100 μg/ml, 24 hours). Orbital fibroblasts without any interventions served as the Control group. No significant differences were observed between Control group and Gyps group (all $P > 0.05$). H_2O_2 (5 μM, 24 hours) treatment significantly increased the protein level of p-ERK, HO-1, and Nrf2 ($P < 0.0001$). Gyps (100 μg/ml, 24 hours) further enhanced these protein levels ($P < 0.05$). *$P < 0.05$, ***$P < 0.001$, ****$P < 0.0001$, compared to the H_2O_2 group. Gyps, gypenosides; TAO, thyroid-associated ophthalmopathy; Nrf2/ERK/HO-1, nuclear factor erythroid 2-related factor 2 (Nrf2)/extracellular signal-regulated kinase (ERK)/heme oxygenase 1 (HO-1); ERK, extracellular-regulated kinase; p-ERK, phosphorylation-extracellular signal-regulated kinase; HO-1, heme oxygenase 1; Nrf2, nuclear factor erythroid 2-related factor 2.

For the autophagy-related signaling (**Figure 6**), H_2O_2 stimulation significantly increased the protein levels of microtubule-associated protein light chain 3 (LC3) and microtubule-associated protein Beclin1 (BECN1) ($P < 0.0001$), while decreasing the expression of p62 ($P < 0.0001$). However, Gyps pretreatment markedly decreased LC3 and BECN1 protein expressions ($P < 0.0001$), while increasing p62 protein expression ($P < 0.0001$).

Gyps alleviated orbital tissue pathologic changes in the TAO animal model

To evaluate the protective effects of Gyps in vivo, orbital tissues from TAO model mice were analyzed histologically. H&E staining showed pronounced inflammatory cell infiltration in the orbital tissue of TAO model mice compared to the control mice. In contrast, Gyps treatment markedly reduced inflammatory infiltration, with a more pronounced effect observed in the high-dose Gyps group (50 mg/kg) (**Figure 7A**).

Masson's trichrome staining demonstrated extensive collagen fiber deposition in the intermuscular and connective tissue regions of orbital tissues in the TAO model group. Gyps pre-treatment significantly attenuated collagen deposition in a dose-dependent manner (**Figure 7B**).

Consistently, immunohistochemical analysis showed that the expression levels of Nrf2 and HO-1 were increased in the orbital tissues of TAO model mice compared with controls, and Gyps pre-treatment enhanced their expression. Meanwhile, the expression of the myofibroblast marker α-SMA was markedly reduced following Gyps treatment (**Figure 8**). These *in vivo* findings are consistent with the anti-inflammatory and anti-fibrotic effects observed *in vitro*.

Discussion

In this study, we found that Gyps modulate the Nrf2/ERK/HO-1 signaling pathway in OFs under oxidative stress induced by low concentrations of H_2O_2. Upon oxidative stress stimulation, ERK is activated through phosphorylation

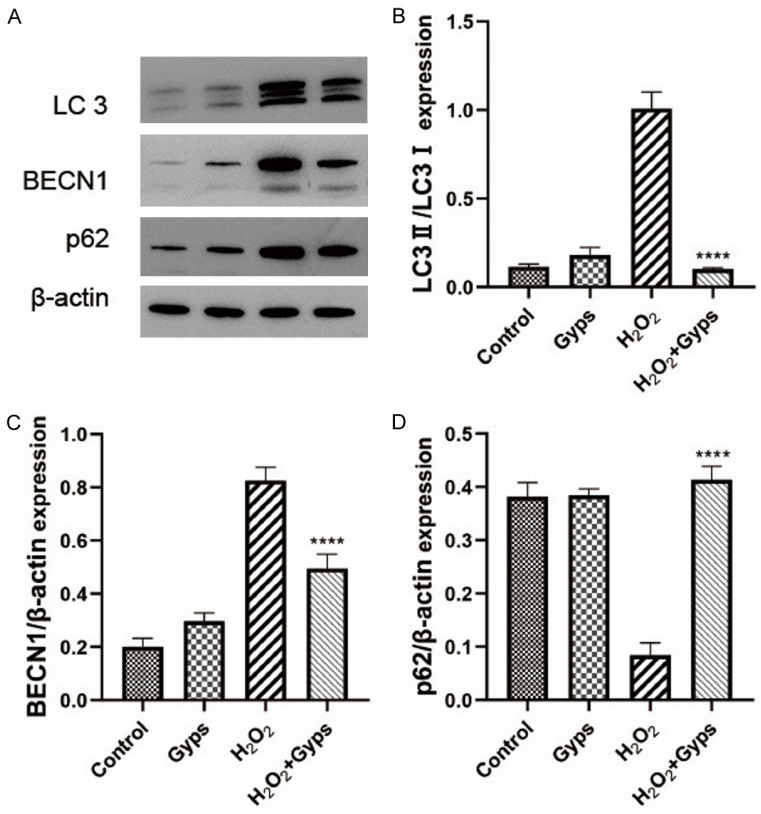

Figure 6. Gyps regulated expression of autophagy-related proteins in orbital fibroblasts of TAO patients. (A) Representative blot images of LC3, BECN1, and p62. (B) Quantitative analysis of LC3. (C) Quantitative analysis of BECN1. (D) Quantitative analysis of p62. OFs of TAO patients (n = 4) were treated with H_2O_2 (5 μM, 24 hours) in the absence or presence of Gyps pretreatment (100 μg/ml, 24 hours). Orbital fibroblasts without any interventions served as the Control group. No significant differences were observed between Control group and Gyps group (all $P > 0.05$). H_2O_2 treatment significantly increased the level of LC3 (B) and BECN1 (C) protein and decreased the level of p62 protein (D) ($P < 0.0001$). Gyps pretreatment significantly decreased LC3 (B) and BECN1 (C) protein levels and increased the level of p62 protein (D) ($P < 0.0001$). ****$P < 0.0001$, compared with H_2O_2 group. Gyps, gypenosides; TAO, thyroid-associated ophthalmopathy; OFs, orbital fibroblasts; LC3, microtubule-associated protein light chain 3; BECN1, microtubule-associated protein Beclin1.

(p-ERK), which in turn promotes the activation and nuclear translocation of Nrf2. Once in the nucleus, Nrf2 binds to the antioxidant response element (ARE), leading to the upregulation of downstream antioxidative genes, including HO-1, thereby enhancing cellular antioxidant capacity and reducing ROS accumulation. With the attenuation of oxidative stress, the expression of autophagy-related markers in OFs decreases, and the local inflammatory factors, including IL-1, IL-6, IFN-γ, TNF-α, Col-1, and α-SMA, showed a downward trend (**Figure 9**).

Network pharmacology offers a powerful and innovative approach to elucidate the complex pharmacologic mechanisms of plant-derived compounds and traditional herbal medicines [32, 33]. This approach not only bridges traditional empirical knowledge with modern pharmacologic research but also provides a robust framework for identifying novel therapeutic strategies for complex diseases. In this study, network pharmacology analysis further supported the mechanistic involvement of oxidative stress-related pathways in the protective effects of Gyps, thereby reinforcing the experimental findings.

H_2O_2 has been used as a well-established inducer of oxidative stress in diverse experimental models, and ROS are recognized as the major cellular oxidative stressors [34, 35]. H_2O_2 may exert bidirectional effects on OFs in a concentration-dependent manner. At concentrations exceeding 5 μM, H_2O_2 exhibits clear cytotoxicity. On the contrary, at concentrations ≤ 5 μM, the cytotoxicity of H_2O_2 is minimal but sufficient to trigger oxidative stress, thereby indirectly promoting inflammatory responses and extracellular matrix production in OFs [36]. H_2O_2 exposure leads to excessive ROS generation in OFs, which subsequently stimulates the production of pro-inflammatory cytokines, including IL-1β and TGF-β1. With increasing ROS levels, OF proliferation also increases in a dose-dependent manner [37]. IL-1β further induces the secretion of downstream inflammatory mediators (e.g., IL-6, IL-8, TNF-α and MCP-1), thereby amplifying local inflammation [38, 39]. Meanwhile, TGF-β1 promotes the trans-differentiation of OFs into myofibroblasts, enhances the synthesis of extracellular matrix components (e.g., HA, FN and Col-1), exacerbates

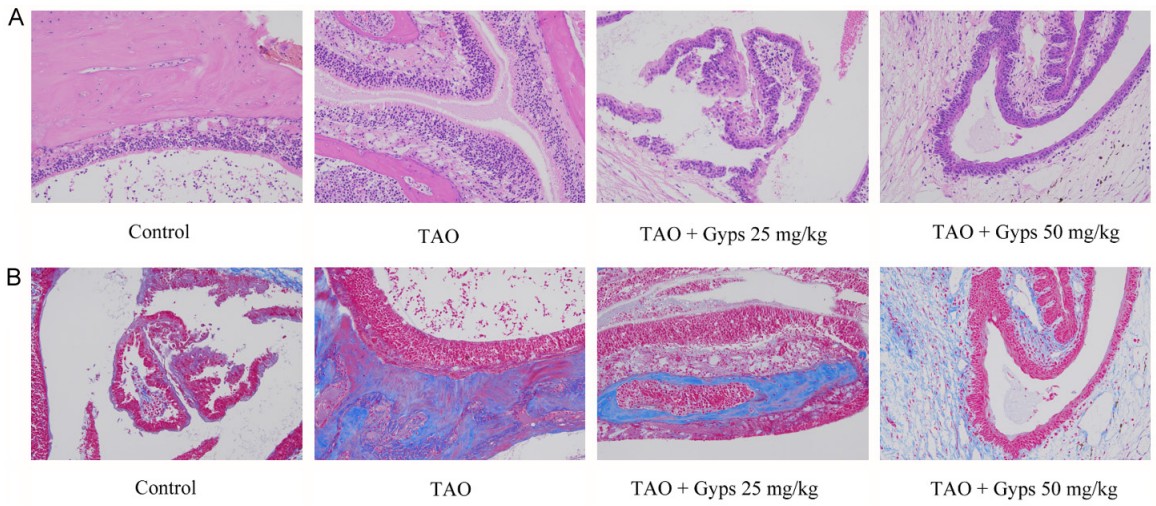

Figure 7. H&E and Masson's trichrome staining of orbital tissues. A. H&E staining: Compared with the control group, the orbital tissues of mice in the TAO model group showed extensive inflammatory cell infiltration. This infiltration was significantly reduced in the Gyps pretreatment groups, particularly in the high-dose group (50 mg/kg). B. Masson's trichrome staining: Extensive blue collagen fiber deposition was observed in the intermuscular spaces and connective tissues of the orbital tissue in the model group. Gyps pretreatment alleviated this fibrotic lesion in a dose-dependent manner.

extraocular muscle fibrosis, ultimately facilitating OF proliferation and fibrotic remodeling [40]. In this study, H_2O_2 stimulation promoted ROS production in OFs, and pretreatment with Gyps increased the secretion of SOD and reduced ROS production. In addition, H_2O_2 exposure elevated the secretion of inflammatory factors and extracellular matrix components, effects that were effectively suppressed by Gyps pre-treatment. These results suggest that OFs are sensitive to oxidative stress induced by H_2O_2 and sensitive to the protective effect of Gyps.

The concentrations of Gyps and H_2O_2 employed in this study were carefully determined based on preliminary experiments and consistency with the existing literature. The 5 μM H_2O_2 concentration we employed is well below levels that typically induce direct cytotoxicity (usually > 100 μM), allowing us to mimic a persistent, low-level oxidative stress microenvironment characteristic of TAO pathology rather than inducing acute injury. This concentration is consistent with the range (1-10 μM) widely adopted in previous OF studies to establish oxidative stress models [36, 37]. Similarly, the 100 μg/ml Gyps concentration selected for this experiment falls within the safe window identified by CCK-8 assays and was demonstrated to most effectively counteract H_2O_2-induced inflammation and fibrosis. This concentration is also comparable to concentrations (25-200 μg/ml) reported in prior studies demonstrating significant antioxidant and anti-inflammatory effects of Gyps in human cell lines, including hepatic stellate cells and endothelial cells [17, 19]. Collectively, these considerations support the biological relevance and methodologic reliability of our experimental design.

In our study, OFs pretreated with Gyps exhibited significantly increased SOD activity and decreased ROS, malondialdehyde (MDA) and lactate dehydrogenase (LDH) following low-concentration H_2O_2 stimulation, compared with cells without Gyps preconditioning. These findings indicate that Gyps exerts a substantial antioxidative effects in OFs derived from patients with and without TAO. Previous studies have demonstrated that Gyps ameliorate cognitive impairment in animal models by enhancing antioxidant capacity and reducing lipid peroxidation [41]. In addition, Gyps exhibits neuroprotective antioxidant effects in *in vitro* models of Parkinson's disease [42]. These studies, together with our data, confirm the antioxidant function of Gyps across different tissues and pathologic conditions.

Previous studies have shown that Gyps can inhibit inflammation both *in vitro* and *in vivo*.

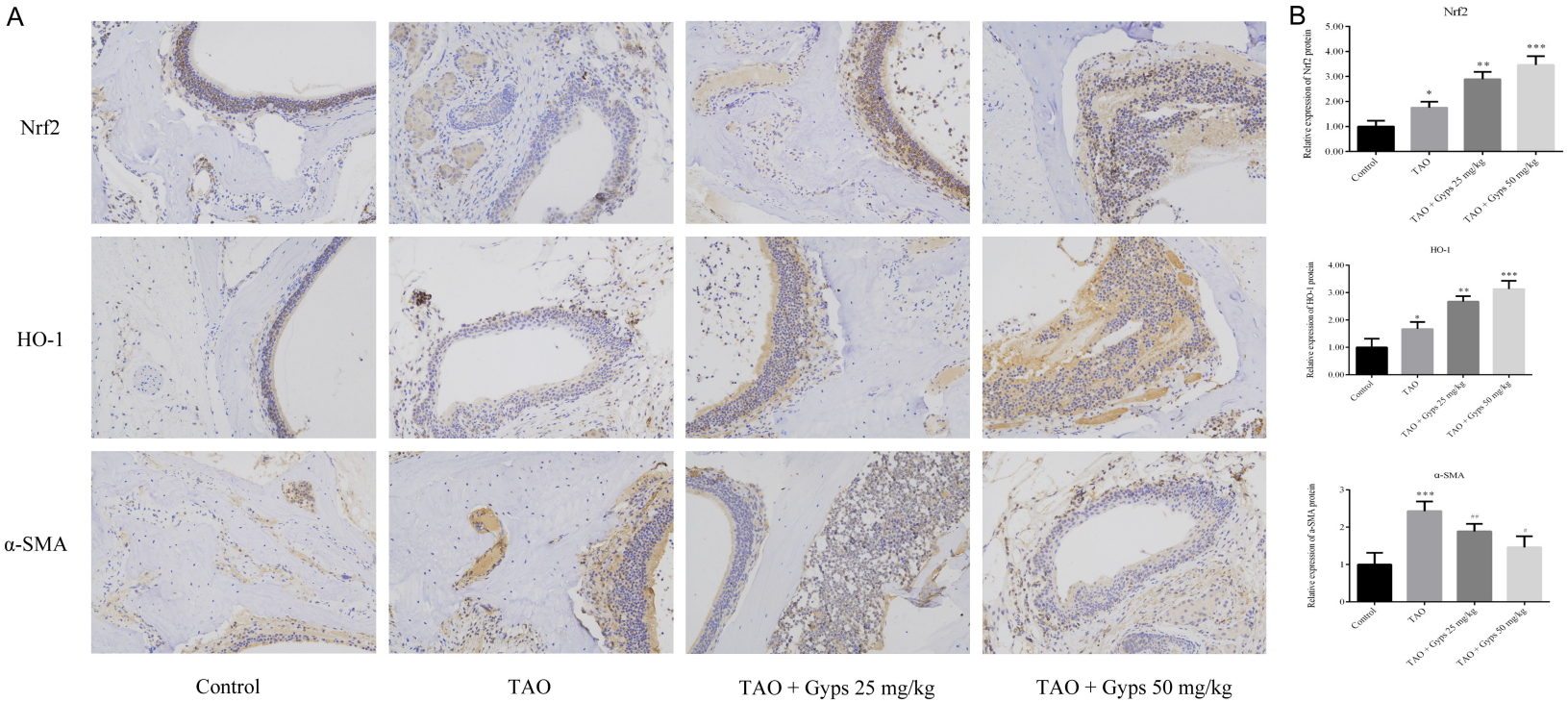

Figure 8. Immunohistochemistry of Nrf2, HO-1, and α-SMA. A. Immunohistochemical staining images. B. Relative protein expression levels. *P < 0.05, **P < 0.01, ***P < 0.001, compared to the control group; #P < 0.05, ##P < 0.01, compared to the TAO model group.

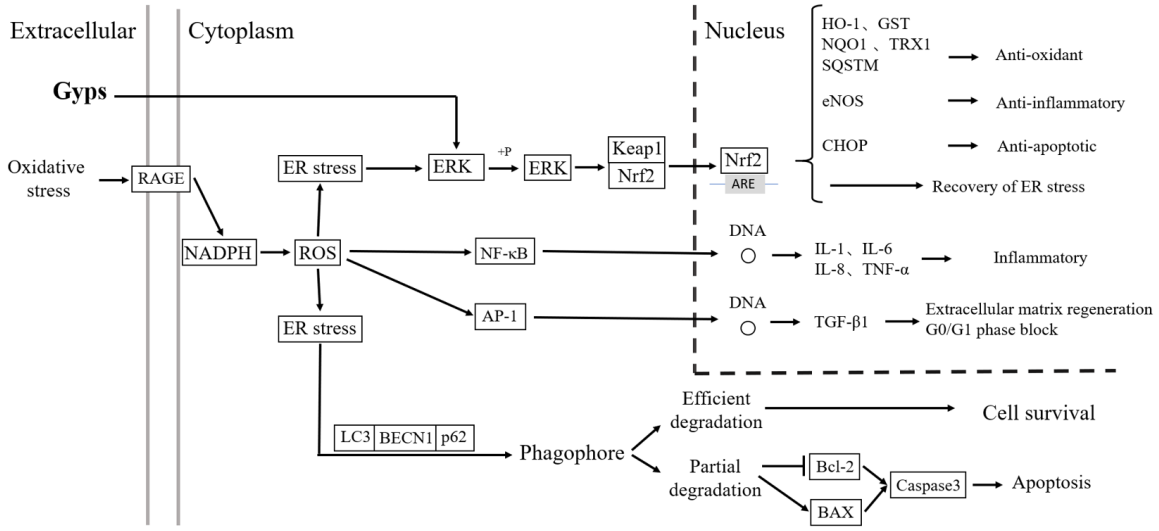

Figure 9. Schematic illustration of the protective effects of Gyps against oxidative stress in TAO. Oxidative stress increases the production of ROS, thereby disrupting the interaction between Nrf2 and its repressor Keap1, facilitating Nrf2 accumulation in the cytoplasm and subsequent translocation into the nucleus. As an antioxidant, Gyps enhance the endogenous activation of the Nrf2 pathway by promoting the dissociation of Nrf2 from Keap1, which increases nuclear localization of Nrf2 under oxidative stress conditions. Activated Nrf2 binds to ARE and induces the transcription of downstream cytoprotective genes, including HO-1, NQO1 and eNOS, thereby attenuating oxidative stress. Consequently, the reduction in oxidative stress suppresses inflammation, fibrosis, and autophagy in orbital tissues. Gyps, gypenosides; TAO, thyroid-associated ophthalmopathy; ROS, reactive oxygen species; Nrf2, nuclear factor erythroid 2-related factor 2; Keap1, kelch-like ECH-associated protein-1; ARE, antioxidant response element; HO-1, heme oxygenase-1, NQO1, NAD(P)H quinone dehydrogenase 1, eNOS, endothelial nitric oxide synthase.

Proinflammatory cytokines and chemokines are produced primarily through activation of the nuclear factor kappa B (NF-κB) signaling pathway [43]. Moreover, Gyps may regulate local inflammatory process in TAO through the STAT Signaling Pathway, thereby contributing to disease control and progression attenuation [44]. This study investigated the role of Gyps in regulating oxidative stress in both TAO and non-TAO OFs. The Nrf2/ERK signaling pathway plays a central role in cellular antioxidant defense mechanisms [45, 46]. ERK, a key member of the mitogen-activated protein kinase (MAPK) family, plays a role in regulating cellular responses to oxidative stress across multiple cell types [47]. Nrf2 is a major leucine zipper transcription factor that responds to alterations in the redox microenvironment and drives the transcription of cytoprotective and antioxidant genes. In nonoxidative-stress, cells, the negative regulator of Nrf2 is Keap1 [48]. Under basal conditions, Nrf2 is sequestered in the cytoplasm through its association with Kelch-like ECH-associated protein 1 (Keap1), which maintains Nrf2 in an inactive state [48]. However, upon exposure to oxidative stress, Nrf2 undergoes phosphorylation at specific serine or threonine residues, dissociates from Keap1, and translocates into the nucleus, to initiate antioxidant gene expression [49, 50]. Moreover, previous studies have shown that ERK signaling can induce Nrf2 activation and regulate the production of SOD, which plays a protective role in oxidative stress [51]. In line with these findings, our results showed that Gyps significantly enhanced ERK activation and then upregulated the expression of Nrf2 to reinforce antioxidant defenses in OFs.

The role of autophagy in regulating inflammatory responses is multifaceted and context-dependent, exerting both inhibitory and stimulatory effects under different conditions. For instance, inhibition of autophagy by 3-methyladenine (3-MA) has been shown to promote IL-1β secretion in bone marrow-derived dendritic cells, while simultaneously inhibiting the production of IL-6 and TNF-α in bone marrow-derived macrophages [52]. In addition, pharmacologic inhibition of autophagy has been reported to reduce IFN-α production in bone marrow cells [53]. Conversely, treating adipo-

cytes with 3-MA further enhances palmitic acid-induced expression of IL-6 and monocyte chemotactic protein-1 (MCP-1) [54]. Moreover, inflammatory cytokines themselves can reciprocally regulate autophagy. Cytokines such as IL-2, IFN-γ, IL-6, TNF-α, IL-1 and TGF-β have been shown to induce among autophagy, whereas classic h2-type cytokines, including IL-13 and IL-4, generally exert inhibitory effects on autophagic activity [55]. This study showed that the expression of key autophagy-related proteins, LC3 II and BECN1, was markedly elevated, while p62 protein was reduced in H_2O_2-stimulated OFs, suggesting enhanced autophagic flux. These findings indicate that autophagy activation is involved in H_2O_2-induced inflammation and fibrosis in OFs. Importantly, Gyps pretreatment reduced LC3 II and BECN1 expression while restoring p62 expression, indicating that Gyps can regulate ROS-induced autophagy in OFs.

In summary, H_2O_2 stimulation promoted ROS production in OFs, and pretreatment with Gyps increased SOD activity, reduced ROS production, and suppressed the secretion of inflammatory factors and extracellular matrix. These antioxidation, anti-inflammatory, and anti-fibrotic effects were observed in H_2O_2-stimulated TAO and non-TAO OFs and were further corroborated by our *in vivo* TAO animal model. Mechanistically, Gyps appears to restore the intracellular redox balance by enhancing antioxidant defenses and regulating autophagy-related protein expression, thereby inhibiting oxidative stress-driven inflammation and fibrosis. This consistency from the cellular to the animal level substantially enhances the reliability of our conclusions and establishes a solid foundation for subsequent clinical research. Further research is required to elucidate the clinical applicability of Gyps, including its pharmacokinetics, bioavailability, and optimal dosage for effective delivery to orbital fibroblasts *in vivo*.

Conclusion

This study provided compelling preclinical evidence supporting Gyps as a potential adjunctive therapy for thyroid-associated ophthalmopathy. By directly targeting OFs, Gyps exert antioxidative, anti-inflammatory, and anti-fibrotic effects through activation of the Nrf2/ERK/HO-1 signaling pathway in both *in vitro* and *in vivo* models. Current first-line treatments, such as corticosteroids and immunosuppressive agents, although effective in suppressing inflammation, are limited by variable responsiveness, disease recurrence, and significant adverse effects [56]. Given the limitations of current first-line treatments, the multi-target regulatory properties of Gyps may offer therapeutic advantages. These findings highlight the translational potential of Gyps for improving disease control and long-term outcomes in TAO patients.

Acknowledgements

This study was supported by the Joint construction project of Henan Medical Science and technology (No. LHGJ20220370), the Natural Science Foundation of Henan (No. 232300420237), the National Natural Science Foundation of China (No. 81360152), the Natural Science Foundation of Guangxi Province (No. 2018GXNSFAA281234), the Henan Province Science and Technology Research Project (No. 252102310020), the National Natural Science Foundation of China (No. 82501355), and the National Natural Science Foundation of China (No. 82160206).

Disclosure of conflict of interest

None.

Address correspondence to: Kaijun Li, Department of Ophthalmology, The First Affiliated Hospital of Guangxi Medical University, No. 6 Shuangyong Road, Qingxiu District, Nanning 530021, Guangxi Zhuang Autonomous Region, China. E-mail: lkj3118lkj@aliyun.com; Chao Ma, Department of Ophthalmology, The First Affiliated Hospital of Zhengzhou University, No. 1 Jianshe East Road, Erqi District, Zhengzhou 450052, Henan, China. E-mail: gmchao219@163.com

References

[1] Luo Y, Yin J, Cao J, Xie B, Zhang F, Ouyang S, Zhou J, Tan Y and Xiong W. Targeted delivery of CD34 aptamer-coupled tocilizumab microspheres for effective treatment of thyroid-associated ophthalmopathy. Invest Ophthalmol Vis Sci 2025; 66: 57.

[2] Liao K, Wei X, Chen Y, Meng D, Mo S, Sun Z, Song F, Lu L and Huang W. Development and validation of a nomogram prediction model for

factors influencing 131I-refractory Graves' hyperthyroidism. Front Endocrinol (Lausanne) 2025; 16: 1628226.
[3] Wu Y, Zhang J, Deng W, Mo C, Liang Y, Huang K, Xu F and Tang F. Comparison of orbital fibroblasts from Graves' ophthalmopathy and healthy control. Heliyon 2024; 10: e28397.
[4] Smith TJ. Controversies surrounding IGF-I receptor involvement in thyroid-associated ophthalmopathy. Thyroid 2025; 35: 232-244.
[5] Liu R, Xin X, Ma S, Guo J, Wu C, Qi X and Luo B. Epac1 inhibits orbital fibroblast activation to ameliorate thyroid-associated orbitopathy-like features through the JAK/STAT signaling pathway. Invest Ophthalmol Vis Sci 2025; 66: 68.
[6] Dik WA, Virakul S and van Steensel L. Current perspectives on the role of orbital fibroblasts in the pathogenesis of Graves' ophthalmopathy. Exp Eye Res 2016; 142: 83-91.
[7] Park M, Banga JP, Kim GJ, Kim M and Lew H. Human placenta-derived mesenchymal stem cells ameliorate orbital adipogenesis in female mice models of Graves' ophthalmopathy. Stem Cell Res Ther 2019; 10: 246.
[8] Liu SY, Wang H, Wang T, Zhou LF, Xu XL, Hou B, Yang B, Sun LS, Pang H, Wang HH and Chen J. METTL3 overexpression and ATF6 silencing-induced Inhibition in HAS2 expression relieves PDGF-BB stimulation-induced HA production and the proliferation of human orbital fibroblasts in graves' ophthalmopathy. J Endocrinol Invest 2025; 48: 2337-2350.
[9] Wang BW, Zhu R, Jin Y, Ouyang X, Jiang FG and Wang XH. Cerium oxide nanoparticles attenuates fibrosis and inflammation in thyroid-associated ophthalmopathy via JNK pathway. Front Mol Biosci 2025; 12: 1580062.
[10] Ciarmatori N, Quaranta Leoni F and Quaranta Leoni FM. Redefining treatment paradigms in thyroid eye disease: current and future therapeutic strategies. J Clin Med 2025; 14: 5528.
[11] van Steensel L, Paridaens D, van Meurs M, van Hagen PM, van den Bosch WA, Kuijpers RW, Drexhage HA, Hooijkaas H and Dik WA. Orbit-infiltrating mast cells, monocytes, and macrophages produce PDGF isoforms that orchestrate orbital fibroblast activation in Graves' ophthalmopathy. J Clin Endocrinol Metab 2012; 97: E400-8.
[12] Xie M, Wang B, Chen J, Wang Y, Rong Y, Su Z, Jiang F and Wang X. Investigating the effects of dendrobine on fibrosis and inflammation in orbital fibroblasts of thyroid-associated ophthalmopathy via network pharmacology, molecular docking, and transcriptomics. Eur J Pharmacol 2025; 1002: 177871.
[13] Jaikampan K, Poomanee W, Thavanapong T, Chittasupho C, Jantadee K and Sainakham M. Preparation of gynostemma pentaphyllum extracts using natural deep eutectic solvents with ultrasound-assisted extraction for cosmetic applications. Plants (Basel) 2025; 14: 1622.
[14] Jiang Q, Yang T, Yang H, Chen Y, Xiong Y, Qin L, Zhang Q, Tan D, Wu X, Zhao Y, Xie J and He Y. Integrated multi-omics investigation of Gypenosides' mechanisms in lowering hepatic cholesterol. Biomolecules 2025; 15: 1205.
[15] Zhang M, Jiang Y, Lu P, Shen Z, Gao X and Wang X. Gypenosides ameliorate hyperlipidemia by activating lipophagy through modulation of the AMPK/mTOR/ULK1 signaling pathway. J Agric Food Chem 2025; 73: 21842-21856.
[16] Li Y, Ren Y, Liu R, Xu W and Gong Y. Alleviation of gypenosides on peripheral and central fatigue via anti-inflammation, anti-oxidation and neurotransmitter regulation. Food Sci Nutr 2025; 13: e70436.
[17] Liu Y, Mao H, Sha Z, Zhao J, Cai H, Xi R, Zhao Z, Yin X, Yang L and Liu C. Gypenoside XLIX inhibiting PI3K/AKT/FOXO1 signaling pathway mediated neuronal mitochondrial autophagy to improve patients with ischemic stroke. Front Pharmacol 2025; 16: 1600435.
[18] Ye Q, Zhu YI, Ye S, Liu H, She X, Niu Y and Ming Y. Gypenoside attenuates renal ischemia/reperfusion injury in mice by inhibition of ERK signaling. Exp Ther Med 2016; 11: 1499-1505.
[19] Megalli S, Davies NM and Roufogalis BD. Anti-hyperlipidemic and hypoglycemic effects of Gynostemma pentaphyllum in the Zucker fatty rat. J Pharm Pharm Sci 2006; 9: 281-291.
[20] Circosta C, De Pasquale R and Occhiuto F. Cardiovascular effects of the aqueous extract of Gynostemma pentaphyllum Makino. Phytomedicine 2005; 12: 638-643.
[21] Liu Y, Li Y, Li J, Rao H, Sun J, Xiu J and Wu N. Gypenosides alleviate oxidative stress in the hippocampus, promote mitophagy, and mitigate depressive-like behaviors induced by CUMS via SIRT1. J Ethnopharmacol 2025; 337: 118823.
[22] Wong WY, Lee MM, Chan BD, Ma VW, Zhang W, Yip TT, Wong WT and Tai WC. Gynostemma pentaphyllum saponins attenuate inflammation in vitro and in vivo by inhibition of NF-κB and STAT3 signaling. Oncotarget 2017; 8: 87401-87414.
[23] Ma C, Li H, Liu W, Lu S, Li X, Chen J, Li K and Wang W. Therapeutic effect of gypenosides on antioxidant stress injury in orbital fibroblasts of Graves' orbitopathy. J Immunol Res 2022; 2022: 4432584.
[24] Khan NM, Haseeb A, Ansari MY, Devarapalli P, Haynie S and Haqqi TM. Wogonin, a plant derived small molecule, exerts potent anti-inflam-

matory and chondroprotective effects through the activation of ROS/ERK/Nrf2 signaling pathways in human Osteoarthritis chondrocytes. Free Radic Biol Med 2017; 106: 288-301.
[25] Ru J, Li P, Wang J, Zhou W, Li B, Huang C, Li P, Guo Z, Tao W, Yang Y, Xu X, Li Y, Wang Y and Yang L. TCMSP: a database of systems pharmacology for drug discovery from herbal medicines. J Cheminform 2014; 6: 13.
[26] Liu X, Ouyang S, Yu B, Liu Y, Huang K, Gong J, Zheng S, Li Z, Li H and Jiang H. PharmMapper server: a web server for potential drug target identification using pharmacophore mapping approach. Nucleic Acids Res 2010; 38: W609-614.
[27] Wang X, Pan C, Gong J, Liu X and Li H. Enhancing the enrichment of pharmacophore-based target prediction for the polypharmacological profiles of drugs. J Chem Inf Model 2016; 56: 1175-83.
[28] Wang X, Shen Y, Wang S, Li S, Zhang W, Liu X, Lai L, Pei J and Li H. PharmMapper 2017 update: a web server for potential drug target identification with a comprehensive target pharmacophore database. Nucleic Acids Res 2017; 45: W356-W360.
[29] Huang da W, Sherman BT and Lempicki RA. Bioinformatics enrichment tools: paths toward the comprehensive functional analysis of large gene lists. Nucleic Acids Res 2009; 37: 1-13.
[30] Huang da W, Sherman BT and Lempicki RA. Systematic and integrative analysis of large gene lists using DAVID bioinformatics resources. Nat Protoc 2009; 4: 44-57.
[31] Bartalena L, Baldeschi L, Dickinson A, Eckstein A, Kendall-Taylor P, Marcocci C, Mourits M, Perros P, Boboridis K, Boschi A, Currò N, Daumerie C, Kahaly GJ, Krassas GE, Lane CM, Lazarus JH, Marinò M, Nardi M, Neoh C, Orgiazzi J, Pearce S, Pinchera A, Pitz S, Salvi M, Sivelli P, Stahl M, von Arx G and Wiersinga WM; European Group on Graves' Orbitopathy (EUGOGO). Consensus statement of the European Group on Graves' orbitopathy (EUGOGO) on management of GO. Eur J Endocrinol 2008; 158: 273-285.
[32] Lin F, Zhang G, Yang X, Wang M, Wang R, Wan M, Wang J, Wu B, Yan T and Jia Y. A network pharmacology approach and experimental validation to investigate the anticancer mechanism and potential active targets of ethanol extract of Wei-Tong-Xin against colorectal cancer through induction of apoptosis via PI3K/AKT signaling pathway. J Ethnopharmacol 2023; 303: 115933.
[33] Wang C, Liu X and Guo S. Network pharmacology-based strategy to investigate the effect and mechanism of α-solanine against glioma. BMC Complement Med Ther 2023; 23: 371.
[34] Zhu YL, Huang J, Chen XY, Xie J, Yang Q, Wang JF and Deng XM. Senkyunolide I alleviates renal Ischemia-Reperfusion injury by inhibiting oxidative stress, endoplasmic reticulum stress and apoptosis. Int Immunopharmacol 2022; 102: 108393.
[35] Jomova K, Raptova R, Alomar SY, Alwasel SH, Nepovimova E, Kuca K and Valko M. Reactive oxygen species, toxicity, oxidative stress, and antioxidants: chronic diseases and aging. Arch Toxicol 2023; 97: 2499-2574.
[36] Berrino E, Guglielmi P, Carta F, Carradori S, Campestre C, Angeli A, Arrighi F, Pontecorvi V, Chimenti P, Secci D, Supuran CT and Gallorini M. In vitro CO-releasing and antioxidant properties of sulfonamide-based CAI-CORMs in a H2O2-stimulated human achilles tendon-derived cell model. Molecules 2025; 30: 593.
[37] Hei X, Lin B, Wu P, Li X, Mao Z, Huang S, Zhang F, Zhou M, Ke Y, Yang H and Huang D. Lutein targeting orbital fibroblasts attenuates fibrotic and inflammatory effects in thyroid-associated ophthalmopathy. Exp Eye Res 2023; 232: 109515.
[38] Chen B, Tsui S and Smith TJ. IL-1 beta induces IL-6 expression in human orbital fibroblasts: identification of an anatomic-site specific phenotypic attribute relevant to thyroid-associated ophthalmopathy. J Immunol 2005; 175: 1310-1319.
[39] Hwang CJ, Afifiyan N, Sand D, Naik V, Said J, Pollock SJ, Chen B, Phipps RP, Goldberg RA, Smith TJ and Douglas RS. Orbital fibroblasts from patients with thyroid-associated ophthalmopathy overexpress CD40: CD154 hyperinduces IL-6, IL-8, and MCP-1. Invest Ophthalmol Vis Sci 2009; 50: 2262-2268.
[40] Chen Q, Pan Y, Hu Y, Chen G, Chen X, Xie Y, Wang M, Li Z, Huang J, Shi Y, Huang H, Zhang T, Wang M, Zeng P, Wang S, Chen R, Zheng Y, Zhong L, Yang H and Liang D. An L-type calcium channel blocker nimodipine exerts anti-fibrotic effects by attenuating TGF-β1 induced calcium response in an in vitro model of thyroid eye disease. Eye Vis (Lond) 2024; 11: 37.
[41] Zhang GL, Deng JP, Wang BH, Zhao ZW, Li J, Gao L, Liu BL, Xong JR, Guo XD, Yan ZQ and Gao GD. Gypenosides improve cognitive impairment induced by chronic cerebral hypoperfusion in rats by suppressing oxidative stress and astrocytic activation. Behav Pharmacol 2011; 22: 633-644.
[42] Wang P, Niu L, Gao L, Li WX, Jia D, Wang XL and Gao GD. Neuroprotective effect of gypenosides against oxidative injury in the substantia nigra of a mouse model of Parkinson's disease. J Int Med Res 2010; 38: 1084-1092.
[43] Ping K, Yang R, Chen H, Xie S, Xiang Y, Li M, Lu Y and Dong J. Gypenoside XLIX activates the Sirt1/Nrf2 signaling pathway to inhibit NLRP3

inflammasome activation to alleviate septic acute lung injury. Inflammation 2025; 48: 42-60.
[44] Hai YP, Lee ACH, Chen K and Kahaly GJ. Traditional Chinese medicine in thyroid-associated orbitopathy. J Endocrinol Invest 2023; 46: 1103-1113.
[45] Liu L, Wu W, Li J, Jiao WH, Liu LY, Tang J, Liu L, Sun F, Han BN and Lin HW. Two sesquiterpene aminoquinones protect against oxidative injury in HaCaT keratinocytes via activation of AMPKα/ERK-Nrf2/ARE/HO-1 signaling. Biomed Pharmacother 2018; 100: 417-425.
[46] Liu N, Liang Y, Wei T, Zou L, Huang X, Kong L, Tang M and Zhang T. The role of ferroptosis mediated by NRF2/ERK-regulated ferritinophagy in CdTe QDs-induced inflammation in macrophage. J Hazard Mater 2022; 436: 129043.
[47] Park JI. MAPK-ERK pathway. Int J Mol Sci 2023; 24: 9666.
[48] Adinolfi S, Patinen T, Jawahar Deen A, Pitkänen S, Härkönen J, Kansanen E, Küblbeck J and Levonen AL. The KEAP1-NRF2 pathway: targets for therapy and role in cancer. Redox Biol 2023; 63: 102726.
[49] Luo X, Wang Y, Zhu X, Chen Y, Xu B, Bai X, Weng X, Xu J, Tao Y, Yang D, Du J, Lv Y, Zhang S, Hu S, Li J and Jia H. MCL attenuates atherosclerosis by suppressing macrophage ferroptosis via targeting KEAP1/NRF2 interaction. Redox Biol 2024; 69: 102987.
[50] Suzuki T, Takahashi J and Yamamoto M. Molecular Basis of the KEAP1-NRF2 Signaling Pathway. Mol Cells 2023; 46: 133-141.
[51] Arthur R, Navik U and Kumar P. Artemisinin ameliorates the neurotoxic effect of 3-nitropropionic acid: a possible involvement of the ERK/BDNF/Nrf2/HO-1 signaling pathway. Mol Neurobiol 2025; 62: 3583-3600.
[52] Cao Y, Xiong J, Guan X, Yin S, Chen J, Yuan S, Liu H, Lin S, Zhou Y, Qiu J, Wang D, Liu B and Zhou J. Paeoniflorin suppresses kidney inflammation by regulating macrophage polarization via KLF4-mediated mitophagy. Phytomedicine 2023; 116: 154901.
[53] Lee HK, Lund JM, Ramanathan B, Mizushima N and Iwasaki A. Autophagy-dependent viral recognition by plasmacytoid dendritic cells. Science 2007; 315: 1398-1401.
[54] Yin J, Wang Y, Gu L, Fan N, Ma Y and Peng Y. Palmitate induces endoplasmic reticulum stress and autophagy in mature adipocytes: implications for apoptosis and inflammation. Int J Mol Med 2015; 35: 932-940.
[55] Matsuzawa-Ishimoto Y, Hwang S and Cadwell K. Autophagy and Inflammation. Annu Rev Immunol 2018; 36: 73-101.
[56] Kang S, Hamed Azzam S, Minakaran N and Ezra DG. Rituximab for thyroid-associated ophthalmopathy. Cochrane Database Syst Rev 2022; 6: CD009226.

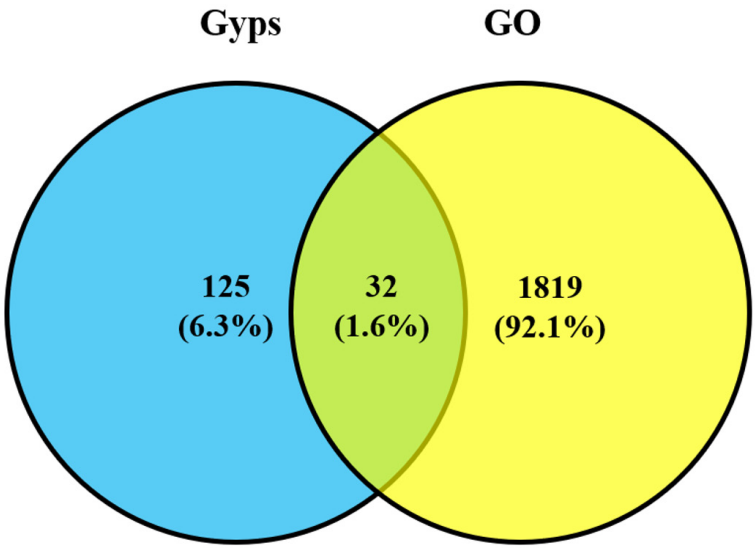

Figure S1. Venn diagram illustrating the respective targets and intersection targets of thyroid-associated ophthalmopathy and gypenosides. Gyps, gypenosides; GO, Gene Ontology.

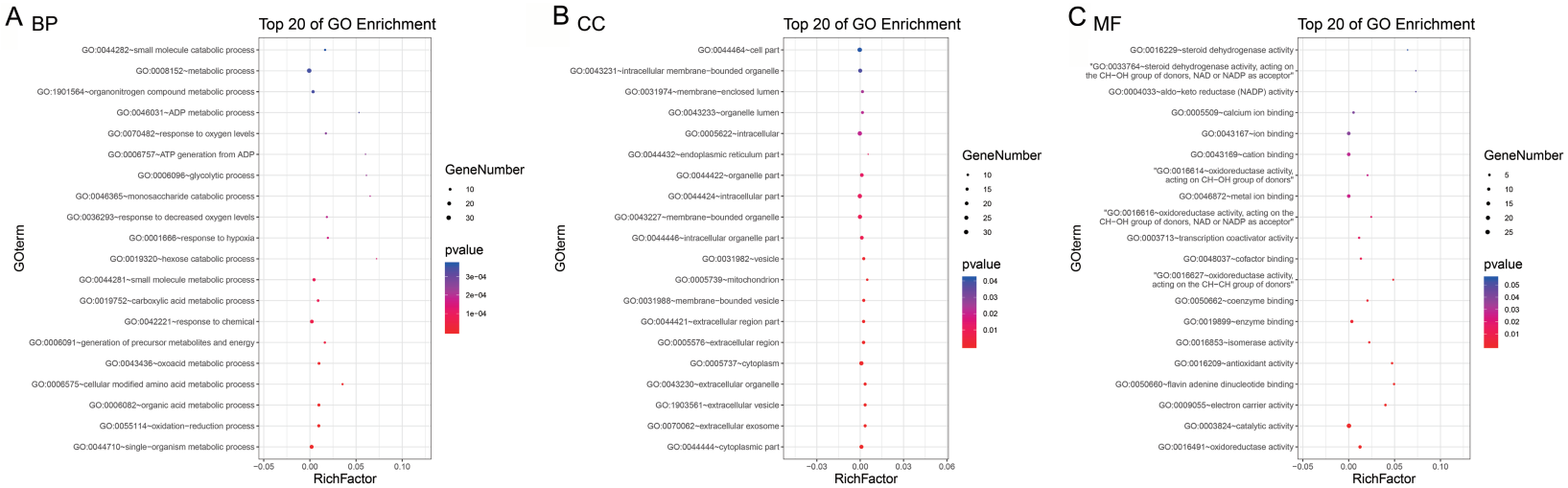

Figure S2. Gene Ontology (GO) enrichment analysis of the intersecting targets between gypenosides and thyroid-associated ophthalmopathy (TAO). The dot size represents the number of related genes, and the color of the dot reflects the corresponding *P* value. A. Biological process (BP). B. Cell component (CC). C. Molecular function (MF). The rich factor represents the ratio of the number of target genes enriched in a given GO term to the total number of background genes annotated to that term.

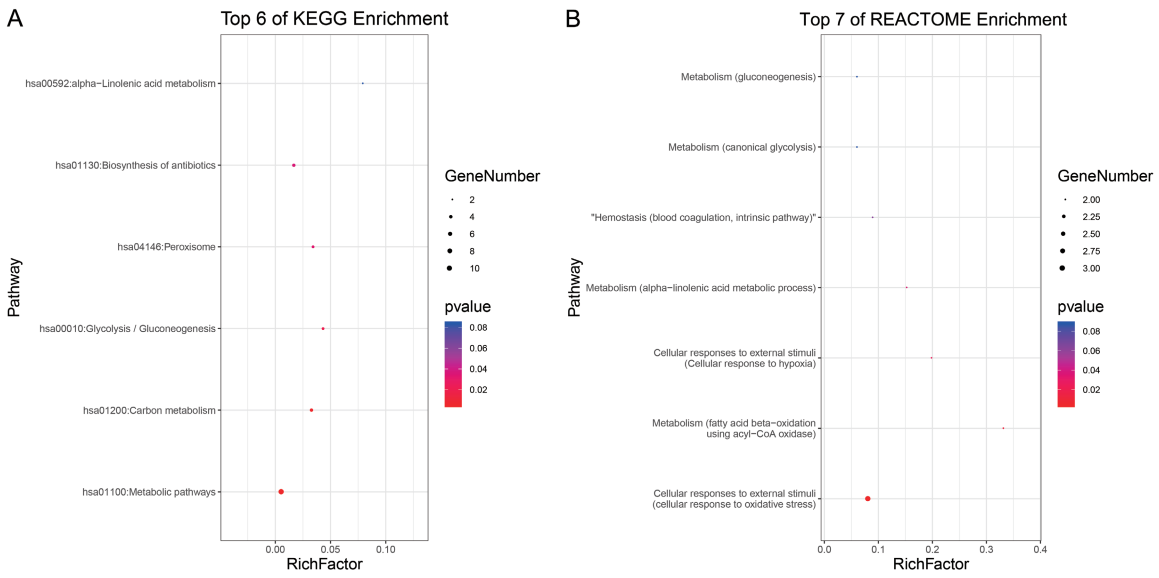

Figure S3. Pathway enrichment analysis of intersection targets using Kyoto Encyclopedia of Genes and Genomes (KEGG) pathways analysis (A) and REACTOME pathway analysis (B). The dot size represents the number of related genes, and the color of the dot reflects the corresponding *P* value. The rich factor represents the ratio of the number of target genes involved in a given pathway to the total number of background genes annotated to that pathway.

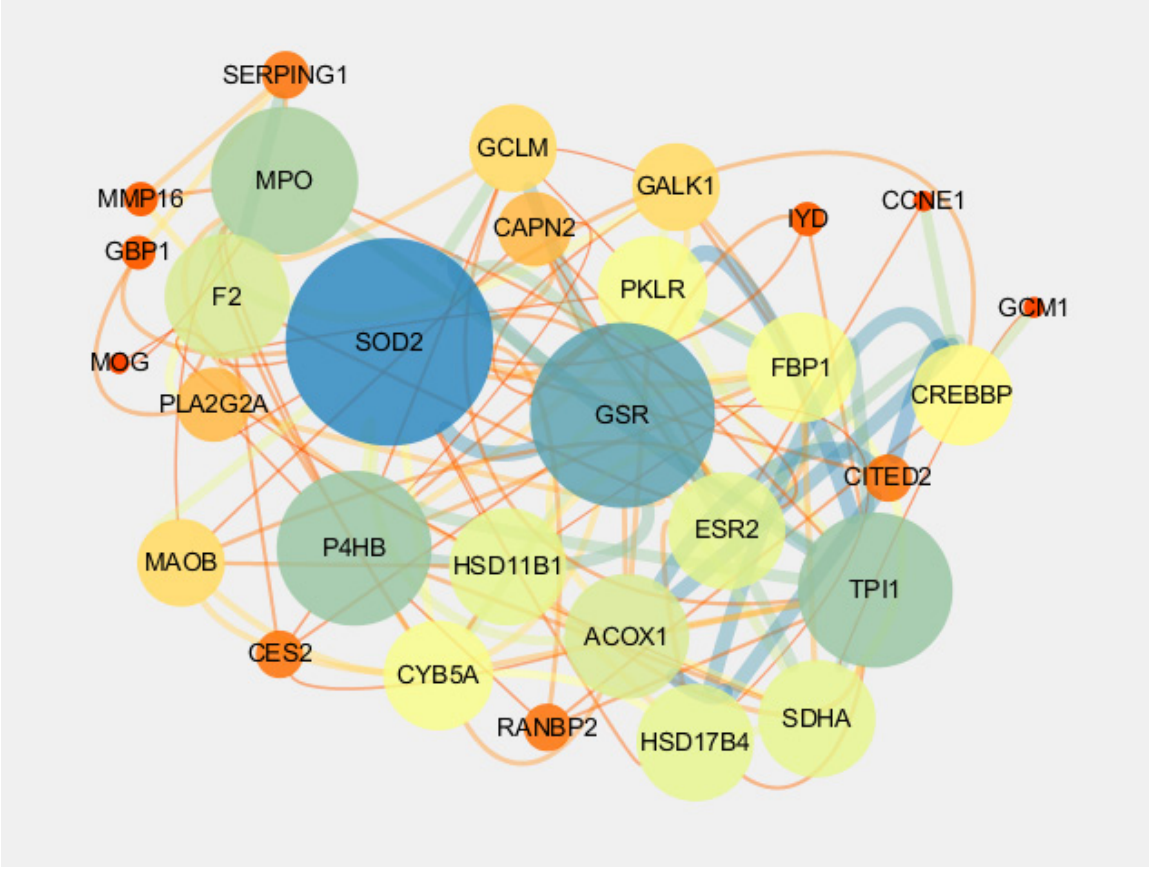

Figure S4. Construction of protein-protein interaction network of proteins expressed by intersection targets. The node size and its color represent the degree, and the edge size and its color represent the comprehensive score. The data was from STRING database.